

Autonomous movement of a chemically powered vesicleShivam Gupta,^{1,*} K. K. Sreeja,^{2,†} and Snigdha Thakur^{1,‡}¹*Department of Physics, Indian Institute of Science Education and Research Bhopal, Bhopal, India*²*Department of Physics, Indian Institute of Technology Madras, Chennai, India*

(Received 1 June 2015; published 7 October 2015)

We investigate the diffusio-phoretic motion of a deformable vesicle. A vesicle is built from the linked catalytic and noncatalytic vertices that consumes fuel in the environment and utilize the resulting self-generated concentration gradient to exhibit propulsive motion. Under nonequilibrium conditions it is found that the self-propulsion velocity of the vesicle depends on its shape, which in turn is controlled by the bending rigidity of the membrane and solvent density around it. The self-propulsion velocity of the vesicle for different shapes has been calculated and the factors which affect the velocity are identified.

DOI: [10.1103/PhysRevE.92.042703](https://doi.org/10.1103/PhysRevE.92.042703)

PACS number(s): 87.17.Jj, 83.80.Lz, 87.16.D–

I. INTRODUCTION

Nondiffusive transport of biological objects such as vesicles and molecular motors as well as nonbiological entities like colloids and aggregates are widely studied both experimentally and theoretically [1–6]. What is most important for these small length scale objects for motility is some degree of spacial or temporal asymmetry. In the biological context, a significant amount of work has been done on cell motility with the motivation to understand the mechanism of cell propulsion, which could then lead to motility modification, i.e., to make it move slower or faster. Chemotaxis and haptotaxis are the widely known mechanisms of cell migration, where the organism exhibits a directed motion with the help of the chemical concentration gradient and adhesive molecules, respectively [1,7]. Modeling cell motility and shape changes is an extremely challenging task due to its inherent complexity, and hence a simpler model for a membranous object, a vesicle, has been adopted for such studies.

In this spirit we study the propulsion of a model vesicle, which is driven by a chemical reaction on its surface. Simplicity of the model makes it feasible for its realization in experiments, and the correlation of the shape change and migration speeds can be probed easily in terms of the physico-chemical parameter.

Inspired by nature, synthetic structures have been designed that use chemical, light, or other forms of energy to perform directed motion [5]. Among the various strategies that are followed for designing such motors, one route is where the propulsion relies on asymmetric chemical reactivity on the surface of the motor, be it bimetallic nanorods [8,9], Janus particles [10,11], or sphere dimer motors [12,13]. The above cited example of asymmetric self-propelled objects assumes that the particle shape is unchanged during the motion. However, in reality many self-propelled objects may change their shape depending on the velocity, environment, or interaction with other objects. Recently there have been

reports of autonomous propulsion for deformable objects with a propulsive effect created by the physical asymmetry [14–16]. Ohta and coworkers have theoretically investigated the individual and collective motion of deformable objects exhibiting self-propulsion [15,17] and showed a bifurcation from a straight line to a circular motion for an isolated particle. A very recent and interesting work by Wilson and colleagues has experimentally demonstrated the autonomous movement of platinum-loaded stomatocytes [14]. These polymeric analogs of liposomes are created by the diblock copolymers and exhibit a remarkably high average directed velocity even in the presence of a small amount of fuel, which is why they can be seen as ideal drug delivery devices.

Here we illustrate the self-propulsion of a chemo-mechanically active vesicle with self-diffusiophoresis as the underlying mechanism and investigate the effect of shape change on the propulsion of such a deformable object. The chemically powered propulsive motion was obtained by the discrete surface model of a vesicle with localized asymmetric catalytic reactions. The vesicle consists of linked catalytic (C) and noncatalytic (N) vertices, which then are immersed in a solvent containing reactive A species. An irreversible reaction $A + C \rightarrow B + C$ takes place at all the catalytic vertices, which in turn gives rise to the nonequilibrium gradient of the B species. The combination of nonequilibrium gradients and potential asymmetry gives rise to the directed motion, similar to nanodimers [13]. We show that at short times, the vesicle moves predominantly in a directed way which then changes to a random walk at longer times. Here we discuss the factors that control the vesicle motility and discuss the shapes of vesicles which will lead to sufficiently large directed velocities. Such directed motion is essential for the applications where propelled vesicles may possibly be used as a carrier of targeted drug delivery or to perform a specific task in the cellular environment.

The paper is organized as follows. In Sec. II we describe the particle-based mesoscopic model for the vesicle motors and solvent. Section III presents various shapes of vesicles obtained in our model and their propulsion behavior. The efficiency of the vesicle motors of different shapes is discussed in Sec. IV. Finally, the conclusions of our study are presented in Sec. V.

* shivam@iiserb.ac.in

† sreeja@physics.iitm.ac.in

‡ sthakur@iiserb.ac.in

II. SIMULATION MODEL

Self-propulsion of the fluid vesicle is simulated using a mesoscopic approach, which combines a particle-based hydrodynamic model for solvent [18–21] and a mesoscale [22], dynamically triangulated surface model for the membrane [23]. A similar model has been used previously to study the dynamics of fluid vesicle in capillary and shear flows [24,25].

A. Triangulated-surface model for the vesicle

The vesicular membrane is modeled using a dynamic triangulation method [23] in which the continuum surface is replaced by a discretized surface defined by vertices, triangles, and links. A vesicle with spherical topology thus consists of N_v vertices connected by $N_L = 3(N_v - 2)$ links and $N_T = 2(N_v - 2)$ triangles. Such a description of the membrane is extremely useful when only the gross features of the structure and interactions are important. The shape deformations of a vesicle is well explored using the curvature elastic energy given by the Canham Helfrich model [26]:

$$H_c = \frac{\kappa}{2} \int (c_1 + c_2)^2 da, \quad (1)$$

where c_1 and c_2 denote the two principle curvatures and κ is the bending stiffness of the membrane. For the triangulated surface model of vesicle a discretized form of this Helfrich Hamiltonian is used [27].

Unlike in the Monte Carlo simulations of triangulated membrane, vertex points interact through a Stillinger-Weber-type potential [25,28] for bonding the vertices (U_b) and excluded volume interaction (U_{ex}). The attractive bonding potential between the connected vertices is given by

$$U_b(r) = \begin{cases} \frac{\gamma \exp[1/(r_{c0}-r)]}{r_{\max}-r}, & \text{if } r > r_{c0} \\ 0 & \text{if } r \leq r_{c0} \end{cases}, \quad (2)$$

where $r = |\mathbf{r}_{ij}|$ is the bond length between vertices i and j . The repulsive excluded volume interaction is incorporated by

$$U_{ex}(r) = \begin{cases} \frac{\gamma \exp[1/(r-r_{c1})]}{r-r_{\min}}, & \text{if } r < r_{c1} \\ 0 & \text{if } r \geq r_{c1} \end{cases}. \quad (3)$$

We use $r_{\min} = 0.67a_0$ and $r_{\max} = 1.33a_0$ as the minimum and maximum possible distance between vertices, respectively.

The triangulated membrane acquires its lateral fluidity from the bond flip mechanism, where the tethers can be flipped between the two possible diagonals of two adjacent triangles at time interval τ_{BF} [25]. Flipping between the catalytic and noncatalytic part of the vesicle is not allowed.

B. Multiparticle collision dynamics of the solvent

To bridge the large length and timescale gaps in the vesicle dynamics a mesoscopic model for the solvent is required. In multiparticle collision dynamics, the solvent is described by N_s pointlike particles of mass m , moving in the simulation box of size $L_x \times L_y \times L_z$. In this scheme, the evolution consists of a series of streaming and multiparticle collision steps. In the streaming step, the dynamics is evolved by Newton's equations of motion governed by forces determined from the total potential energy $V(\mathbf{r}^{N_v}, \mathbf{r}^{N_s})$ of the system [29].

In the collision steps, which occur at time intervals τ , the pointlike solvent particles are sorted into cubic cells with cell size a_0 . The choice of cell size is such that the mean free path $\lambda < a_0$. Multiparticle collisions among the solvent molecules are performed independently in each cell, which results in the postcollision velocity of solvent particle i in cell ξ being given by $\mathbf{v}'_i = \mathbf{V}_\xi + \hat{\omega}_\xi(\mathbf{v}_i - \mathbf{V}_\xi)$, where \mathbf{V}_ξ is the center-of-mass velocity of particles in cell ξ and $\hat{\omega}_\xi$ is a rotation matrix. In order to ensure Galilean invariance for systems with small λ , a random grid shift is applied in each direction of the simulation box [30]. The method described above conserves mass, momentum, and energy and accounts for the hydrodynamic interactions and fluid flow fields [18,19], which are important for the dynamics of the active fluid vesicle.

C. Membrane and solvent interaction

Theoretical descriptions of the vesicle motion arise from self-diffusiophoresis [2,13,31], which in this case is based on phoretic motion of the vesicle in an external inhomogeneous chemical field. To model this, initially the vesicle is immersed in a fluid with N_s solvent particles of kind A . We randomly pick a patch of membrane with connected vertices which are labeled catalytic (C), and these vertices are chemically active. The rest of the membrane vertices are considered to be noncatalytic (N) or chemically inactive. We start with a catalytic patch that is nearly circular in shape, and this shape can fluctuate as the patch diffuses on the vesicle surface. Since the flip move at the boundary of the patch is restricted, single catalytic vertices cannot be detached from the patch, and the diffusion of the entire patch is only possible.

A chemical reaction $A + C \rightarrow B + C$ takes place only on the catalytic vertices C whenever the solvent A comes within the Lennard-Jones (LJ) cutoff distance. This localized reaction produces an inhomogeneous concentration of solute molecules around the vesicle, which in turn is responsible for the propulsion of vesicle (see Fig. 1). However, the fluid inside the vesicle consists of only A -type particles, and no chemical

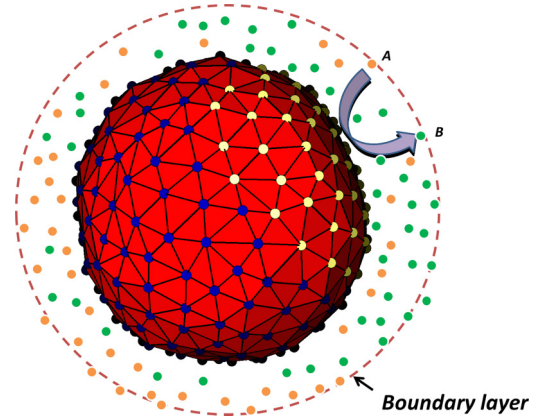


FIG. 1. (Color online) A chemically active vesicle composed of catalytic (yellow) and noncatalytic (blue) vertices. The figure depicts the chemical reaction that leads to conversion of fuel A (orange) to product B (green) molecule within the boundary layer, hence producing the inhomogeneous distribution of chemical species. The boundary layer around the vesicle within which the intermolecular forces act is also shown.

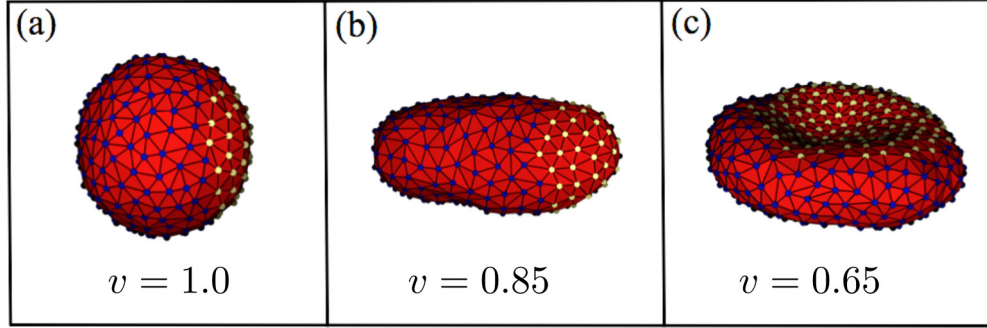


FIG. 2. (Color online) Shapes of membrane vesicle with the corresponding reduced volume v ; (a) sphere, (b) ellipsoid, and (c) discoid.

reaction takes place for inside fluid. The A and B solvent molecular species interact with all the vesicle vertices through repulsive LJ potentials,

$$V_{\beta S}(r) = 4\epsilon_{\beta} \left[\left(\frac{\sigma}{r} \right)^{12} - \left(\frac{\sigma}{r} \right)^6 + \frac{1}{4} \right], \quad r \leq r_c, \quad (4)$$

with the cutoff distance $r_c = 2^{1/6}\sigma$. We use the notation $V_{\beta S}$, where $S = C, N$ and $\beta = A, B$ to denote various interactions between solvent and membrane. In particular, we take $V_{AC} = V_{BC} = V_{AN}$, characterized by the energy and distance parameters ϵ_A and σ , respectively; however, interactions between the N vertex and B molecules, V_{BN} , have energy parameter ϵ_B . Hence the B molecules produced in the reaction on a catalytic sphere react differently with catalytic and noncatalytic monomers, and this asymmetry is an important element in the self-propulsion mechanism for the vesicle [13]. The above mentioned potential ensures that the fluid particles will not escape or enter the vesicle in the time scale of interest. In order to mimic the fluxes of reactive species into and out of the system to drive it out of equilibrium and lead to establishment of a nonequilibrium steady state, B molecules are converted back to A molecules when they diffuse far away from the vesicle.

The time evolution of the system is governed by hybrid molecular dynamics-multiparticle collision dynamics [18].

D. Simulation parameters

Other simulation details are as follows: all quantities are reported in dimensionless LJ units based on energy ϵ_A , mass m , and distance σ parameters and $\sigma = a_0$. The vesicle moves in a solvent of A and B molecules within a cubic box of volume V and linear dimension $30a_0$ with periodic boundary conditions. The MPC rotation angle was fixed at $\phi = 90^\circ$. The average number density of the solvent outside the vesicle was kept at $\rho_{\text{out}} \approx 10$, whereas the inside solvent number density ρ_{in} was varied from 1 to 10 to vary the shape of the vesicle. The masses of both A and B species are $m = 1$, and the masses of the membrane vertices were adjusted according to their diameters, $d_v = 2a_0$, to ensure the density matching between vertex and solvent. The system temperature was fixed at $k_B T = 0.26\epsilon_A$. Newton's equation of motion is integrated using the velocity Verlet algorithm, with the MD time step $\Delta t = 0.005$. The MPC time interval is $\tau = 0.25$, and the time interval for the bond flip is $\tau_{\text{BF}} = 0.1$. We have probed various sizes of the vesicle where N_v varies from 110 to 677. Unless specified, the value

of $\kappa = 5\epsilon_A$, $\gamma = 80\epsilon_A$, and the LJ parameter $\epsilon_B = 0.01\epsilon_A$. For the bond and excluded volume interaction, we use the cutoff lengths $r_{c0} = 1.15a_0$ and $r_{c1} = 0.85a_0$.

III. MEMBRANE VESICLE PROPULSION

We investigate the self-propulsion of vesicle of different shapes: spherical, ellipsoidal, and discoidal vesicles. These various shapes are generated by changing the number of the solvent particle density enclosed by the vesicle, which in turn affect the area-to-volume ratio leading to a shape transformation [32]. The shapes of the vesicle described in the study and the corresponding reduced volumes v are shown in Fig. 2, where $v = \frac{V_{\text{ves}}}{4\pi R_0^3/3}$, R_0 being the radius of a sphere with the same surface area as that of the vesicle and V_{ves} is the volume of the vesicle. We obtain a spherical vesicle with $v = 1$ when the density of the solvent inside and outside of the vesicle are equal. On reducing the inside solvent density we get the prolate or ellipsoidal shape with reduced volume $v = 0.85$, and further reduction results in discocytes with $v = 0.65$.

A. Spherical vesicle

The self-propulsion of a membrane vesicle occurs as a result of the nonequilibrium concentration gradient produced by the chemical reaction at the catalytic vertices of the vesicle, in conjunction with the different intermolecular forces between the A and B chemical species and the vertices. See Movie 1 in Ref. [33] for the dynamics of a propelling spherical vesicle. The ability of the self-propelled vesicle to execute directed motion is determined by monitoring the mean value of the center of mass velocity of the vesicle motor, projected along the axis between the center of mass of the vesicle to the center of mass of catalytic vertices: $V_z = \langle \langle \mathbf{V}(t) \cdot \hat{\mathbf{R}}(t) \rangle \rangle$, where the double angular bracket denotes the average over time and realizations. $\hat{\mathbf{R}}(t)$ is the unit vector along this axis. An isolated vesicle motor undergoes self-propelled motion in the given direction with average directed velocity $\langle V_z \rangle$; however, such small motors are also subjected to strong thermal fluctuation that lead to a distribution of propagation velocities. This distribution has been shown to be closely approximated by a Boltzmann distribution [13] with mean $\langle V_z \rangle$. The magnitude and nature of the directed motion is strongly influenced by the vesicle solvent interactions and the percentage fraction of total vertex that is catalytic (C_f). Figure 3 shows the normalized

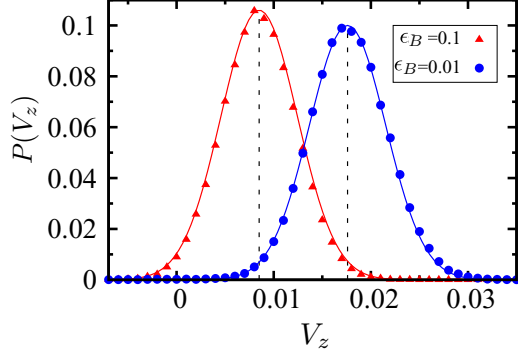


FIG. 3. (Color online) Plot of $P(V_z)$, the probability density of V_z for vesicle with $N_v = 302$ and $\epsilon_A = 1.0$. Solid lines represent Maxwell Boltzmann fit to data, and dashed lines correspond to the mean value of the distribution showing $\langle V_z \rangle = 0.0085$ for $\epsilon_B = 0.1$ and $\langle V_z \rangle = 0.0176$ for $\epsilon_B = 0.01$.

probability distribution $P(V_z)$ for the system with $N_v = 302$ with $C_f = 25\%$ for different values of energy parameter ϵ_B .

As stated before asymmetry is a crucial component for the self-propulsion for the vesicle, and in this case asymmetry is supplied by the existence of a strong product molecule B concentration gradient and difference in interaction potential of the product B molecule with catalytic and noncatalytic vertex. In Fig. 3 we calculate the average directed velocity of the vesicle $\langle V_z \rangle$ for interaction potential strength $\epsilon_B = 0.01$ and 0.1 keeping $\epsilon_A = 1.0$. The figure clearly illustrates better propulsion for a larger difference of the interaction strength, i.e., for higher asymmetry.

Another important element for vesicle propulsion is the local steady state concentration of species B in the vicinity of the catalytic C vertices. In order to have a vesicle with maximum possible directed movement it is important to have an optimum number of catalytic vertices on it. Having too many or too less catalytic vertices will not be able to establish a sufficient nonequilibrium B concentration gradient around the vesicle; hence, directed vesicle propulsion will not be possible. Figure 4(a) shows the average velocity of vesicle $\langle V_z \rangle$ as a function of C_f . From the figure it is clear that $C_f \approx 25\%$ catalytic gives maximum directed velocity $\langle V_z \rangle \approx 0.018$ for $N_v = 302$, comparable to the previously reported sphere dimer motors [34]. This is further supported by higher strength of the local steady state concentration gradient of species B in the vicinity of the catalytic vertices shown in Fig. 4(b), for $C_f = 25\%$ and 50% . In the figure r is the distance of solvent B molecules from the center of mass of catalytic vertices.

The nanoscale objects will not move ballistically in a given direction due to strong fluctuations from surrounding medium [10]. Instead, the motion will be ballistic at short times, but at longer times, the motion will change to a random walk, in which the spans of directed motion will be interrupted by a random change in direction. The effective diffusion coefficient can then be calculated by the velocity autocorrelation function as

$$D_e = \frac{1}{d} \int_0^\infty dt \langle \mathbf{V}(t) \cdot \mathbf{V}(0) \rangle, \quad (5)$$

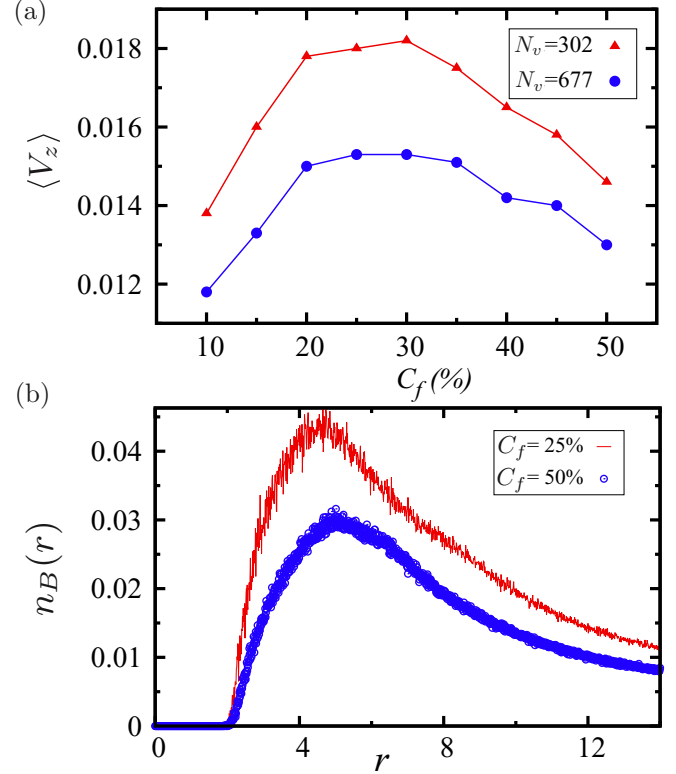


FIG. 4. (Color online) (a) Variation of average directed velocity of the vesicle $\langle V_z \rangle$ as a function of percentage of catalytic vertices C_f for $N_v = 302$ and $N_v = 677$. (b) The local steady state concentration of B particles around the catalytic center of mass, $n_B(r)$, showing larger $n_B(r)$ for $C_f = 25\%$ when compared to $C_f = 50\%$.

where $\mathbf{V}(0)$ is the center of mass velocity of the vesicle motor in d dimensions. The center of mass velocity can be decomposed to the averaged directed velocity in the $\hat{\mathbf{R}}(t)$ direction and fluctuations as $\mathbf{V} = \hat{\mathbf{R}}(t)\langle V_z \rangle + \delta$, giving

$$D_e = D_0 + \frac{1}{d} \langle V_z \rangle^2 \tau_R. \quad (6)$$

The first term on the right-hand side is the diffusion coefficient in absence of any propulsion, and the second term is characterized by the decay of the orientational correlation function with an orientational relaxation time τ_R . The diffusion coefficient can equivalently be determined from the mean square displacement (MSD) $\Delta L^2(t) = \langle |\mathbf{r}_{\text{CM}}(t) - \mathbf{r}_{\text{CM}}(0)|^2 \rangle$ as $D_e = \lim_{t \rightarrow \infty} \Delta L^2(t)/dt$. There are two relevant characteristic time scales in the system [35]. First is the characteristic diffusion time of the product solvent particles around the vesicle given by $\tau_D = R_v/D$, where D is the diffusion coefficient of solvent molecules and R_v is the vesicle size. This time scale sets the relaxation time of the redistribution of the particles around the vesicle when it changes orientation. Second is the orientational relaxation time τ_R which controls the changes in the orientation of the spherical vesicle and is defined via the orientational autocorrelation function: $C_\theta(t) = \langle \hat{\mathbf{R}}(t) \cdot \hat{\mathbf{R}}(0) \rangle \sim e^{-(t/\tau_R)}$. The solvent transport coefficient can be calculated analytically for MPC dynamics [36], giving $\tau_D \approx 600$ for a vesicle with $N_v = 110$.

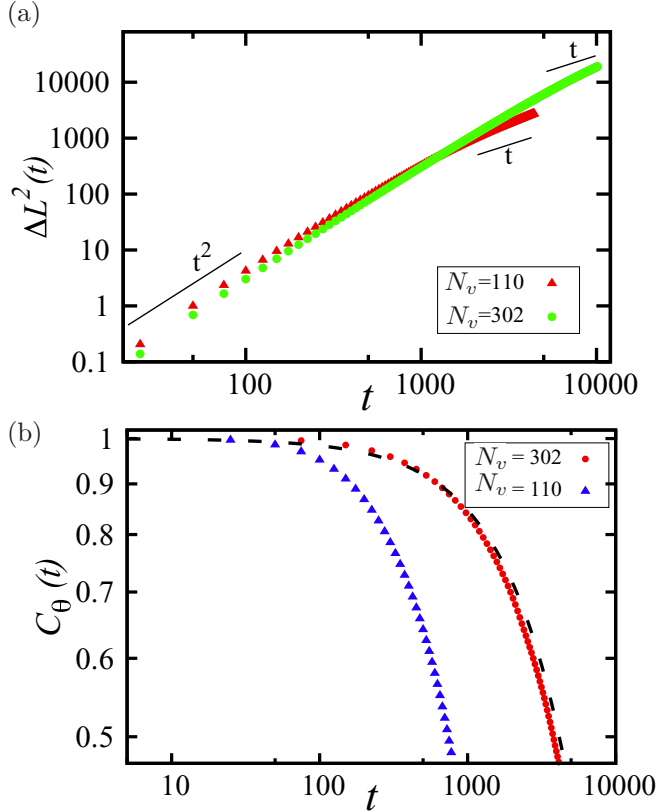


FIG. 5. (Color online) (a) Mean square displacement $\Delta L^2(t)$ for different sized vesicles having $C_f = 25\%$ depicting the ballistic motion $\sim t^2$ at short times and diffusive motion $\sim t$ at long times. (b) Orientational autocorrelation function for two vesicles. The dashed line is an exponential fit to data. Time is in units of MD steps.

For short times ($t \ll \tau_D$) MSD is shown to exhibit a ballistic regime [35] where $\Delta L^2(t) \sim \langle V_z \rangle^2 t^2$, while for long times $t \gg \tau_R$ it exhibits a linear behavior as $\Delta L^2(t) \sim 6(D_0 + \langle V_z \rangle^2 \tau_R/d)t$. Figure 5(a) shows the MSD for the vesicle of different sizes $N_v = 110$ and 302. For a smaller vesicle, fitting of the short and long time of this plot is comparable with the theoretical expression given above to estimate the average vesicle propagation velocity $\langle V_z \rangle$ and reorientation time τ_R and enhanced diffusion coefficient. However, for a larger vesicle with $N_v = 302$ perfect scaling of t has not been observed in our simulation time scale, but a deviation from t^2 at a longer time is clearly visible. Figure 5(b) shows the orientation autocorrelation function for a differently sized vesicle. The corresponding relaxation times along with diffusion coefficients (D_e) and $\langle V_z \rangle$ are given in Table I.

For most of the vesicle sizes reported in Table I we find the diffusion coefficient in the absence of propulsion to be $D_0 \sim 10^{-3}$, whereas the contribution from self-propulsion in D_e is much higher. Consequently the dynamics for these vesicles are dominated by the directed motion. However, as the vesicle size decreases, the directed motion contribution given by $\frac{1}{3}\langle V_z \rangle^2 \tau_R$ keeps decreasing and D_0 starts to play an important role.

TABLE I. The average directed velocity, orientational relaxation time (in units of MD steps), and enhanced diffusion coefficients, obtained from the mean square displacement and orientation auto-correlation function for different sizes of spherical vesicles.

| N_v | $\langle V_z \rangle$ | τ_R | D_e |
|-------|-----------------------|----------|-------|
| 29 | 0.021 | 175 | 0.020 |
| 110 | 0.019 | 1100 | 0.132 |
| 194 | 0.018 | 2500 | 0.270 |
| 302 | 0.017 | 6000 | 0.578 |
| 434 | 0.016 | 11500 | 0.981 |

B. Prolate or ellipsoidal vesicle

Vesicles are highly adaptive structures having a rich diversity of shapes which mainly depends on the temperature, pressure, and bending stiffness [32]. In order to get an insight into the propulsion efficiency of vesicles in various shapes, we induce the shape change either by changing the number density of solvent inside the vesicle, which in turn changes the solvent pressure inside and hence the shape of the vesicle [37], or by varying the bending elasticity and thus the curvature. To evaluate the morphological changes of the vesicle in a quantitative manner, we calculated asphericity α as an order parameter that reflects the deviation from the spherical shape [25]. Asphericity α is obtained from the three eigenvalues ($\lambda_1, \lambda_2, \lambda_3$) of the moment-of-inertia tensor given as $\alpha = \frac{(\lambda_1 - \lambda_2)^2 + (\lambda_2 - \lambda_3)^2 + (\lambda_3 - \lambda_1)^2}{2R_g^4}$, where $R_g^2 = \lambda_1 + \lambda_2 + \lambda_3$. Figure 6(a) shows the increase in asphericity on reducing

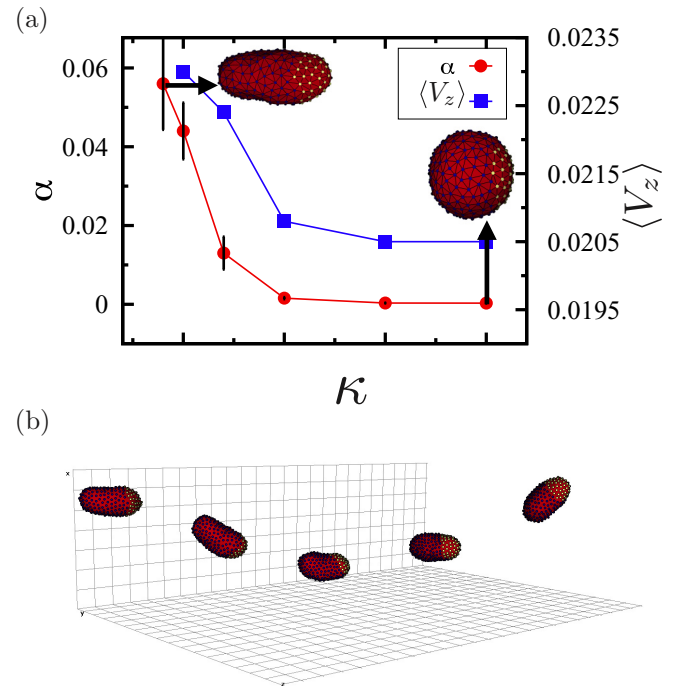


FIG. 6. (Color online) (a) Variation of asphericity α and the average directed velocity $\langle V_z \rangle$ as a function of bending rigidity κ keeping $\rho_{in} = 1$. The fluctuations in the shapes are represented by the error bars shown for α . (b) The propulsion and reorientation of a prolate vesicle.

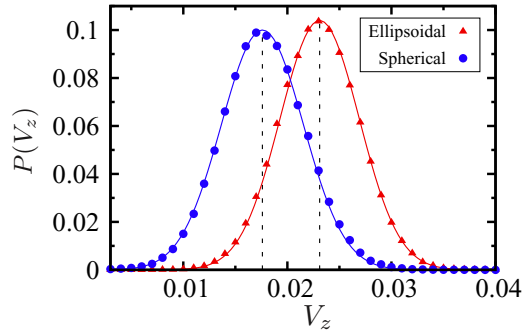


FIG. 7. (Color online) Plot of $P(V_z)$, the probability density of V_z for vesicle with $N_v = 302$ with prolate and spherical shapes. Solid lines are fitted to the Maxwell Boltzmann distribution.

the bending rigidity κ of the vesicle. The observed shape transition in this case is from spherical vesicle to prolate or ellipsoidal vesicle. The surface undulations can cause minor shape fluctuations in vesicles, and this can be seen from the error bars shown for α in Fig. 6(a), with smaller κ having larger fluctuations. It should be noted that unlike the significant shape transition in the case of vesicles under shear flow [25], in the present case of a static fluid we hardly observe any shape transition at a given κ and inside solvent density.

The shape changes in vesicles are accompanied with a strong change in dynamical behavior of the vesicle. See Movie 2 in Ref. [33] for the dynamics of a prolate vesicle. Figure 6(b) shows a motile prolate vesicle which reorients in the course of time due to thermal fluctuation. Figure 7 shows the comparison of the probability distribution of directed propulsive velocity for a spherical and ellipsoidal vesicle. It is quite evident that the prolate or ellipsoidal vesicle has enhanced propulsion velocity, $\langle V_z \rangle = 0.023$, as compared to the spherical shape, $\langle V_z \rangle = 0.017$. It must be noted here the motion of the elliptical vesicle is such that the catalytic vertices are around the tip of the ellipse, and movement is along the long axis. This orientation can be explained in terms of bending energy, which allows the solvent interactions to deform the vesicle such that its movement is carried out with least possible drag.

The strength of the drag force depends not only on the viscosity at low speeds, but also on the cross-sectional shape that is presented to the fluid by the object in its direction of motion. For a rigid spherical object of radius R the drag coefficient is given by Stoke's law as $f_t = 6\pi\eta R$, where η is the viscosity of the medium, whereas for an ellipsoidal case the drag coefficient changes to $f_t = \frac{4\pi\eta a}{\ln(2a/b)-1/2}$ for motion at low speed parallel to the long axis of the ellipsoid [38], where a and b are the semimajor and semiminor axis, respectively. Despite the fact that vesicles are not very rigid objects, we can use the above mentioned drag coefficients in our calculation, because once the directional motion is established, the fluctuations about the mean shape are much less. The calculated drag coefficient for the vesicle having $N_v = 302$ in prolate and spherical shapes is found to be ≈ 98 and 125, respectively.

Does the increased directed velocity of the ellipsoidal vesicle guarantee it to be a better candidate for microscale swimmers than a spherical vesicle? To answer this, next we probed the mean square displacement and orientational angular correlation for the prolate shape and compared it with the sphere.

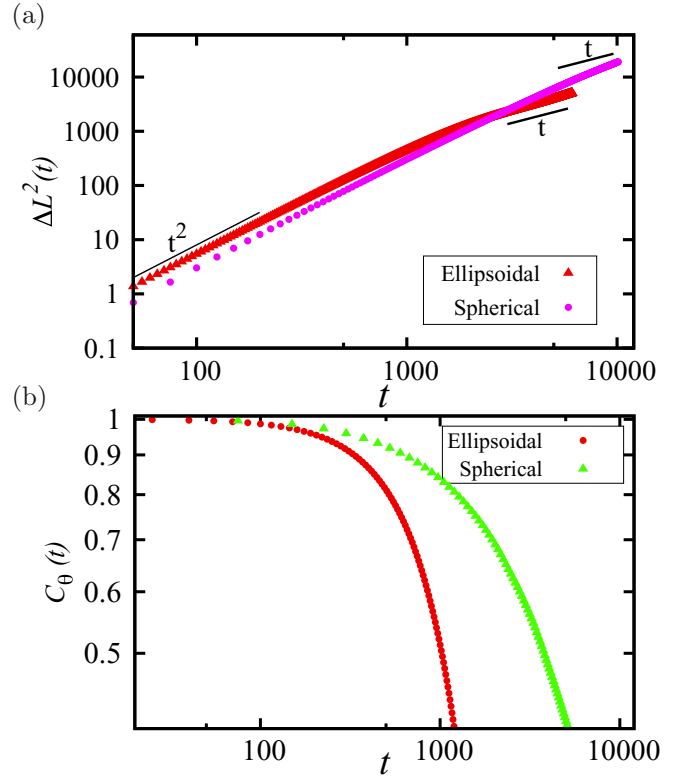


FIG. 8. (Color online) (a) Orientational autocorrelation function as a function of time for ellipsoidal and spherical vesicles having $N_v = 302$. (b) Mean square displacement $\Delta L^2(t)$ for ellipsoidal and spherical vesicles having $N_v = 302$. MSD for the ellipsoidal shape depicts the ballistic motion $\sim t^2$ at short times and diffusive motion $\sim t$ at long times. Time is in units of MD steps.

Figure 8(a) compares the orientational autocorrelation function $C_\theta(t)$ for the two different shapes discussed so far, which can be used to calculate the orientational relaxation time τ_R . The faster decay of the autocorrelation function in the case of ellipsoidal vesicles clearly depicts the faster reorientation of the vesicle in a prolate shape. The relaxation time τ_R for the prolate shape is found to be 1700 MD steps, which is much smaller than the spherical vesicle having same number of vertices. Table I shows the spherical vesicle of $N_v = 302$ has $\tau_R = 6000$ MD steps. Further, the change in directed motion to a random walk at a time scale of τ_R is also shown in Fig. 8(b). The reduction in the reorientation time for an ellipsoidal shape can be explained in terms of the nonrigid nature of the membrane. In the case where the prolate vesicle is a rigid object, the concentration gradient produced by the vesicle which is responsible for the self propulsion would be along the vector $\hat{\mathbf{R}}(t)$ and would be symmetric normal to the vector. However, presence of floppiness breaks this symmetry and induces a force that will lead to reorientation of the vesicle. This symmetry breaking is easier in a prolate shape as compared to a spherical shape, hence it reorients faster.

C. Discocyte vesicle

Here we investigate the propulsion of vesicles having a discocyte shape. See Movie 3 in Ref. [33], which was obtained

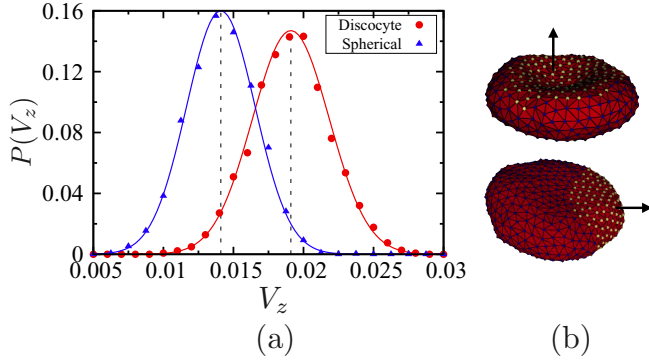


FIG. 9. (Color online) (a) Comparison of $P(V_z)$, the probability density of V_z for vesicle with $N_v = 677$ in a discocyte and spherical shape. (b) Instantaneous configuration of moving discocytes in the face-on and edge-on mode. Arrow shows the direction of movement of the vesicle.

by reducing the number density of the solvent inside the vesicle to $\rho_{in} = 2$. Unlike the case of ellipsoids, where we have a unique mode of propulsion with the velocity direction along its long axis, here we obtain two different modes of propulsion: in one the discocyte moves with its face on, and in the other it moves with its edge at the propelling front. Figure 9(a) shows both propulsion configurations. We observe a lower $\langle V_z \rangle$ for the face-on configuration as compared to the edge-on configuration of the discocyte.

Figure 9(b) compares the directed velocity V_z for the discocyte moving in the edge-on configuration with a spherical vesicle having the same number of vertices $N_v = 677$. It is evident from the plot that the discocytes have higher propulsion with $\langle V_z \rangle = 0.019$ than their spherical counterpart with $\langle V_z \rangle = 0.014$.

IV. VESICLE MOTOR EFFICIENCY

Chemically powered vesicle motors convert chemical energy into mechanical work, driving the self-propelled motion while working in an environment where viscous drag is important. The efficiency η_s of a chemically powered motor, which measures the effectiveness of mechanochemical energy transduction, can be defined as [9]

$$\eta_s = \frac{P_{\text{mech}}}{P_{\text{chem}}}, \quad (7)$$

where P_{mech} is the mechanical power output of the motor and P_{chem} is the total chemical power input to the motor. P_{mech} and P_{chem} are further defined as $P_{\text{mech}} = \zeta \langle V_z \rangle^2$ and $P_{\text{chem}} = \Delta\mu R$, where ζ is the drag coefficient of the vesicle motor, $\langle V_z \rangle$ is the directed propulsion velocity of the vesicle, R is the net chemical reaction rate, and $\Delta\mu$ is the change in the chemical potential in the reaction. To determine the efficiency from above equation, the net chemical reaction rate R was calculated by counting the number of $A \rightarrow B$ reactive events that take place at the catalytic vertices per unit time. In the MPC-MD simulations the change in the chemical potential is given by

$$\Delta\mu = \mu_B - \mu_A = -k_B T \ln \frac{n_B n_A^{\text{eq}}}{n_B^{\text{eq}} n_A}, \quad (8)$$

TABLE II. Comparison of the average directed velocity and Stoke's efficiency for a vesicle motor of various size and shapes. The LJ energy parameter $\epsilon_A = 1.0$.

| N_v | Shape | ϵ_B | $\langle V_z \rangle$ | η_s |
|-------|-------------|--------------|-----------------------|----------|
| 110 | Spherical | 0.01 | 0.019 | 0.0027 |
| 302 | Spherical | 0.01 | 0.017 | 0.0020 |
| 302 | Spherical | 0.1 | 0.008 | 0.0004 |
| 302 | Ellipsoidal | 0.01 | 0.023 | 0.0030 |
| 677 | Discocyte | 0.01 | 0.019 | 0.0015 |
| 677 | Spherical | 0.01 | 0.014 | 0.0012 |

where n_A^{eq} and n_B^{eq} denote the equilibrium number densities of A and B species, respectively, and n_A and n_B are the steady state densities [39]. The drag coefficient depends not only on the viscosity, but also on the cross-sectional shape that is presented to the fluid by the vesicle in its direction of motion. Again to estimate the drag coefficient, we approximate the vesicle to be nearly rigid and hence, for spheres, $\zeta = 6\pi\eta R$, for ellipsoids moving along its long axis $\zeta = \frac{4\pi\eta a}{\ln(2a/b)-1/2}$ and for disks moving edge on $\zeta = \frac{32}{3}\eta p$, where p is the radius of the disk [38]. We compare the Stokes efficiency of the various sizes and shapes of the vesicle in Table II.

It is evident from the above calculation that the power associated with the mechanical work of the motor is larger for smaller vesicles of the same shape, as the Stokes efficiency for the spherical vesicle of $N_v = 110$ is 0.27% and that of a vesicle with $N_v = 302$ is 0.20%. On changing the shape of the vesicle its efficiency also changes. Table II shows that the ellipsoidal motor with $N_v = 302$ is more efficient with $\eta_s = 0.30\%$ than its spherical counterpart with $\eta_s = 0.20\%$. Similarly, comparison of spherical and discocyte shapes shows enhancement of efficiency in the discocyte shape. The maximum efficiency achieved in our simulations is about 0.30%, which is similar to the other chemically powered motors [9,39]; however, this efficiency is much less than that of most nano- and micromotors in biology.

V. CONCLUSION

Investigations of the dynamics of soft deformable self-propelled particles are at an early stage of development. Here we have studied the diffusio-phoretic motion of a chemically powered vesicle, which acquires the motility by creating a gradient of surrounding product solvent molecules. The mesoscopic model for vesicle dynamics discussed in this article provides insight into the factors that control the propulsion.

We show that depending on the bending rigidity and solvent density around the vesicle, different shapes of vesicle can be obtained, and all these shapes exhibit very different dynamical behavior. Our calculations conclude that the directed velocity of the vesicle is maximum for an optimum fraction of catalytic vertices; more or less than that would slow down the dynamics. For a given fraction of catalytic surface, the velocity of the vesicle depends on its shape. We find that a prolate as well as discocyte vesicle exhibit higher directed velocity as compared to a spherical vesicle of same size. However, the prolate shape of the vesicle makes it more prone to the

reorientation due to thermal fluctuation as compared to its spherical counterpart. Having investigated the dynamics of a single vesicle, the natural extension of our study would be to consider the collective dynamics of such deformable objects.

Our approach should be useful for investigation of a biological cell as well as recently studied polymeric vesicles [14]. The potential applications of such vesicle motors will involve launching them to perform a given task, such as cargo transport, and further investigations of interaction between them can provide the information needed to design

motors that can cooperate with each other to perform such tasks.

ACKNOWLEDGMENTS

The work was supported by SERB, India. The computational work was carried out at the HPC facility in IISER Bhopal, India.

S. G. and S. K. K. contributed equally to this work.

-
- [1] I. Cantat and C. Misbah, in *Transport and Structure*, Lecture Notes in Physics Vol. 532 (Springer, Berlin, 1999), pp. 93–136.
- [2] R. Golestanian, T. B. Liverpool, and A. Ajdari, *Phys. Rev. Lett.* **94**, 220801 (2005).
- [3] J. Nardi, R. Bruinsma, and E. Sackmann, *Phys. Rev. Lett.* **82**, 5168 (1999).
- [4] Y. Sumino, N. Magome, T. Hamada, and K. Yoshikawa, *Phys. Rev. Lett.* **94**, 068301 (2005).
- [5] E. R. Kay, D. A. Leigh, and F. Zerbetto, *Angew. Chem. Int. Ed.* **46**, 72 (2007).
- [6] J. L. Anderson, *Phys. Fluids* **26**, 2871 (1983).
- [7] I. Cantat, C. Misbah, and Y. Saito, *Eur. Phys. J. E* **3**, 403 (2000).
- [8] W. F. Paxton *et al.*, *J. Am. Chem. Soc.* **126**, 13424 (2004).
- [9] W. Wang, T.-Y. Chiang, D. Velegol, and T. E. Mallouk, *J. Am. Chem. Soc.* **135**, 10557 (2013).
- [10] J. R. Howse, R. A. L. Jones, A. J. Ryan, T. Gough, R. Vafabakhsh, and R. Golestanian, *Phys. Rev. Lett.* **99**, 048102 (2007).
- [11] M. N. Popescu, S. Dietrich, M. Tasinkevych, and J. Ralston, *Eur. Phys. J. E* **31**, 351 (2010).
- [12] L. F. Valadares *et al.*, *Small* **6**, 565 (2010).
- [13] G. Rückner and R. Kapral, *Phys. Rev. Lett.* **98**, 150603 (2007).
- [14] D. A. Wilson, R. J. M. Nolte, and J. C. M. van Hest, *Nature Chem.* **4**, 268 (2012).
- [15] T. Ohta and T. Ohkuma, *Phys. Rev. Lett.* **102**, 154101 (2009).
- [16] T. Miura *et al.*, *Langmuir* **26**, 1610 (2010).
- [17] A. Menzel and T. Ohta, *Europhys. Lett.* **99**, 58001 (2012).
- [18] R. Kapral, *Adv. Chem. Phys.* **140**, 89 (2008).
- [19] G. Gompper, T. Ihle, D. M. Kroll, and R. G. Winkler, *Adv. Polym. Sci.* **221**, 1 (2009).
- [20] A. Malevanets and R. Kapral, *J. Chem. Phys.* **110**, 8605 (1999).
- [21] A. Malevanets and R. Kapral, *J. Chem. Phys.* **112**, 7260 (2000).
- [22] J.-S. Ho and A. Baumgärtner, *Phys. Rev. Lett.* **63**, 1324 (1989).
- [23] D. Nelson, T. Piran, and S. Weinberg (eds.), *Statistical Mechanics of Membranes and Surfaces*, 2nd ed. (World Scientific, Singapore, 2003).
- [24] H. Noguchi and G. Gompper, *Pub. Natl. Acad. Sci. USA* **102**, 14159 (2005).
- [25] H. Noguchi and G. Gompper, *Phys. Rev. E* **72**, 011901 (2005).
- [26] W. Helfrich, *Z. Naturforsch.* **28**, 693 (1973).
- [27] C. Itzykson, in *Proceedings of the GIFT Seminar, Jaca 85*, edited by J. Abad, M. Asorey, and A. Cruz (World Scientific, Singapore, 1986).
- [28] F. H. Stillinger and T. A. Weber, *Phys. Rev. B* **31**, 5262 (1985).
- [29] D. Sarkar, S. Thakur, Y.-G. Tao, and R. Kapral, *Soft Matter* **10**, 9577 (2014).
- [30] T. Ihle and D. M. Kroll, *Phys. Rev. E* **63**, 020201 (2001).
- [31] R. Golestanian, T. B. Liverpool, and A. Ajdari, *New J. Phys.* **9**, 126 (2007).
- [32] J. Kas and E. Sackmann, *Biophys. J.* **60**, 825 (1991).
- [33] See Supplemental Material at <http://link.aps.org/supplemental/10.1103/PhysRevE.92.042703> for movies showing the propulsion of vesicles. Movie 1, 2 and 3 shows the movement of a spherical, ellipsoidal and discoidal vesicles respectively.
- [34] Y.-G. Tao and R. Kapral, *J. Chem. Phys.* **128**, 164518 (2008).
- [35] R. Golestanian, *Phys. Rev. Lett.* **102**, 188305 (2009).
- [36] S. Thakur and R. Kapral, *Phys. Rev. E* **85**, 026121 (2012).
- [37] X. Li, I. V. Pivkin, H. Liang, and G. E. Karniadakis, *Macromolecules* **42**, 3195 (2009).
- [38] D. Boal, *Mechanics of the Cell* (Cambridge University Press, Cambridge, 2012).
- [39] Y.-G. Tao and R. Kapral, *J. Chem. Phys.* **131**, 024113 (2009).